Ferromagnetism in a graphene nanoribbon with grain boundary defects

Jian Zhou,[1,*] Ting Hu,[2] Jinming Dong,[2,†] and Yoshiyuki Kawazoe[3]

[1]*National Laboratory of Solid State Microstructures and Department of Materials Science and Engineering, Nanjing University, Nanjing 210093, P. R. China*

[2]*Group of Computational Condensed Matter Physics, National Laboratory of Solid State Microstructures and Department of Physics, Nanjing University, Nanjing 210093, P. R. China*

[3]*Institute for Materials Research, Tohoku University, 2-1-1 Katahira Aoba-ku, Sendai, 980-8577 Japan*

(Received 27 January 2012; revised manuscript received 4 June 2012; published 23 July 2012)

A kind of hybrid graphene nanoribbon (GNR) with two different edges (one zigzag and another armchair) has been proposed and studied by first-principles calculations, which could be constructed by different kinds of periodical grain boundaries joining together the normal zigzag and armchair GNRs. It is found that the ground state of hybrid GNR is robustly ferromagnetic (FM) with a high FM Curie temperature, which is totally different from that of the normal GNRs. Most of the hybrid GNRs are found to be FM metal, except for the type-A hybrid GNR with a very narrow width, which contains three pairs of 5-7 topological defects in a unit cell of its grain boundary. A metal-semiconductor transition can be found in the type-A structure when its number of zigzag carbon chains decreases. More interestingly, it is found that all the hybrid GNRs, especially the type-A ones, can become half-metallic, which could be useful in the future applications of spintronics. Finally, the binding-energy calculations for these hybrid GNRs show that they could be stable and possibly synthesized in future experiments. In addition, the study of their edge defect indicates that their ferromagnetism and half-metallicity could survive even in the existence of edge defects.

DOI: 10.1103/PhysRevB.86.035434 PACS number(s): 81.05.ue, 73.22.Pr, 75.75.−c

I. INTRODUCTION

The graphene nanoribbon (GNR) is one of the most interesting carbon materials that has been studied extensively in recent years.[1–3] The GNR can be obtained by unfolding a single-walled carbon nanotube or by cutting a finite-width slice from an infinite graphene plane along a particular direction. However, it shows much different physical properties from the carbon nanotube or graphene, which are caused by its different edges, widths, and chiralities.

The first-principles calculations confirm that all the armchair GNRs are semiconductors, while all the zigzag ones are metallic when the spin polarization is not included. However, a small band gap would be opened in the zigzag GNRs if the spin polarization is taken into account. The local magnetic moments would emerge at two zigzag edges, which are ferromagnetically (FM) coupled in the same edge, but antiferromagnetically (AFM) coupled between two opposite edges.[4–6] The magnetic property in such materials without d-orbital electrons is quite interesting and important in the condensed matter physics because its origin is not very clear at present. Moreover, a lot of researches have been done to tune the magnetic properties of the GNRs and other carbon-based materials. For example, one could get the half-metallicity in the zigzag GNRs by an external electric field or by doping,[7–11] which is quite important in the application of spintronics.

On the other hand, the grain boundaries in the polycrystalline graphene have also been studied intensively in recent years,[12–22] which can change the graphene's electronic properties remarkably. For example, two distinct transport behaviors (high and low transparency) are found in a graphene with different grain boundary structures, which is quite important for graphene's practical application in digital electronic devices.[12] In addition, it is important and interesting to note that the room-temperature FM has been observed experimentally at the grain boundaries of highly oriented pyrolytic graphite.[13]

Recently, Botello-Méndez *et al.* have studied by first-principles calculations the electronic, magnetic, and transport properties of the hybrid graphene and the graphene nanoribbon with periodical grain boundary joining the normal zigzag and armchair GNRs, which contain only one pair of 5-7 topological defects in a unit cell. They found that such hybrid graphene structures can exhibit the half-metallicity and other fascinating electronic and magnetic properties.[14] Since the grain boundary can be used to join two different oriented graphenes together, it can give more freedom to tailor the geometric structure of the hybrid graphene and tune its electronic properties. Many other interesting physical and chemical properties due to the existence of the grain boundary in graphene can be possibly found in future experiments and theories.

In this paper, we have constructed a kind of hybrid GNR with two different types of edges (one armchair and another zigzag), which could be realized by introducing in it a grain boundary parallel to its edges. The electronic and magnetic properties of three types of hybrid GNRs have been studied by first-principles calculations. It is found that the robust ferromagnetism with a high Curie temperature appears in these hybrid GNRs, which is totally different from that of normal GNRs. Also, an interesting half-metallicity is found to exist in all the hybrid GNRs.

The rest of this paper is organized as follows. In Sec. II, the geometric model and computational methods are described. In Sec. III, the main numerical results and some discussions are given. Finally, Sec. IV is the conclusion.

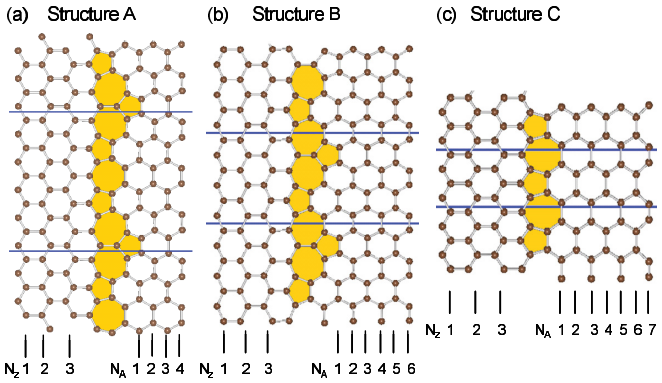

FIG. 1. (Color online) Geometric structures of different hybrid GNRs: (a) type-A structure, GNR-A (3,4); (b) type-B structure, GNR-B (3,6); c) type-C structure, GNR-C (3,7). The orange parts indicate the grain boundary defects. The two blue lines indicate the unit cells along the ribbon's length direction used in our calculations. N_Z and N_A are the numbers of zigzag and armchair carbon chains of the hybrid GNRs in their width directions, respectively.

II. GEOMETRIC MODEL AND COMPUTATIONAL METHODS

A. Geometric model of the hybrid GNRs with different grain boundaries

Three types of hybrid GNRs have been constructed by different periodical grain boundaries, as shown in Fig. 1. For example, the type-A hybrid GNR could be made by three pairs of 5-7 carbon defects in a period of its grain boundary, connecting together its zigzag and armchair edges, as shown in Fig. 1(a). It is a modification of the boundary structure in Ref. 12 with a very small lattice mismatch between its two edges, which can be defined as follows:

$$\eta = \frac{L_z - L_a}{2L_z} \times 100\%. \quad (1)$$

Here, L_z and L_a are the lengths of ideal zigzag and armchair edges without the boundary defect, respectively. As seen from Fig. 1(a), the type-A structure has five hexagons at the zigzag edge and six at the armchair edge in a unit cell along its length direction. Therefore, its $L_z = 5\sqrt{3}a$ and $L_a = 9a$, where a is the C-C bond length. Thus, its lattice mismatch is about -1.96%, where the negative sign means its zigzag edge is elongated and the armchair one is compressed.

The geometrical structure of type-A hybrid GNR can be identified by a pair of integers (n,m), where n and m represent the numbers of zigzag and armchair carbon chains along its width direction, respectively. For example, Fig. 1(a) presents a type-A structure having three zigzag chains at one side and four armchair chains at the other side. Then, its geometrical structure is defined as GNR-A (3,4).

Two other types of hybrid GNRs, i.e., types B and C, are constructed by two and one pair of 5-7 defects in a unit cell, as shown in Figs. 1(b) and 1(c), respectively. Similar to the type-A structure, their geometrical structures can also be defined by a pair of integers (n,m). Therefore, Figs. 1(b) and 1(c) present the GNR-B (3,6) and GNR-C (3,7), respectively, because the former has three zigzag chains and six armchair ones in its width direction, and the latter has three zigzag chains and seven armchair ones. Based upon Eq. (1), the lattice mismatches of the GNR-B (3,6) and GNR-C (3,7) are found to be about -7.74% and 6.70%, respectively, which are much larger than those of GNR-A structure. Here, the positive value of GNR-C (3,7) means that its zigzag edge is compressed and the armchair edge is elongated, which is just opposite to the type-A and -B structures. In this work, it is noted that the type-C GNR has the same structure as the hybrid GNR used in Ref. 14, except that their edges are saturated by hydrogen atoms.

B. Computational method and details

The geometric and electronic structures are calculated by the density functional theory (DFT), implemented by VASP code,[23,24] in which the projected augmented wave method[25,26] and the Perdew-Burke-Ernzerhof exchange correlation are used.[27] The $2s$ and $2p$ orbitals of the carbon atom are treated as valence ones. A large supercell along the ribbon's width direction is used to simulate the isolated one-dimensional hybrid GNR, making the closest distance between two adjacent GNRs to be 10 Å. The ribbon is placed along the x direction, and a large vacuum region is added in both the y and z directions.

The geometric structures of all three types of GNRs are optimized by using the conjugate-gradient algorithm. Both the atomic positions and the lattice constant along the ribbon axis are relaxed and the maximum residual forces on atoms are less than 0.02 eV/Å. We have used an $n_k \times 1 \times 1$ k-points mesh in optimizing the structures and total energy calculation. The n_k is variable for different length GNRs by the formula $n_k \geqslant 50/L_x$, where L_x is the lattice constant in the x direction in units of Å. A much denser k point is used to calculate the band structure.

III. RESULTS AND DISCUSSIONS

A. Type-A structure: Three pairs of 5-7 defects

We first study the electronic properties of type-A structure with three pairs of 5-7 defects in a period of its grain boundary, shown in Fig. 1(a). In order to compare total energies of its FM and AFM configurations, we have also constructed a $2 \times 1 \times 1$ supercell of it during the calculations. This is considered because its original unit cell contains only five atoms in its zigzag edge, which can not form a perfect AFM spin configuration.

It is well known that the magnetic configuration of the normal zigzag GNR is the AFM coupling between its two zigzag edges and the FM one within the same zigzag edge. For the hybrid GNRs, there is only one zigzag edge, which still prefers the FM coupling along its edge rather than the AFM or nonmagnetic one, demonstrated by our DFT calculations. The energy differences between the FM and AFM configurations of four GNR-A structures with different zigzag chain numbers but fixed armchair ones are shown in Table I. It is clearly seen from Table I that for all the calculated GNR-A structures, the FM configurations are almost $0.03 \sim 0.07$ eV per zigzag atom lower in energy than the AFM one, depending on their zigzag chain number, which leads to a high Curie temperature above the room temperature. So, it is obvious that more zigzag chains in the type-A hybrid GNRs benefit their FM configurations.

TABLE I. Energy difference ΔE of the type-A hybrid GNR in the FM and AFM configurations, defined as $\Delta E = E_{\mathrm{FM}} - E_{\mathrm{AFM}}$. $\Delta E/n$ denotes the energy difference per zigzag edge atom, where n is the number of carbon atoms at the zigzag edge in a unit cell. Here, the number of armchair chains is fixed to be four.

Hybrid GNRs	ΔE (eV)	$\Delta E/n$
GNR-A (1,4)	−0.3243	−0.0324
GNR-A (2,4)	−0.5673	−0.0567
GNR-A (3,4)	−0.5344	−0.0534
GNR-A (4,4)	−0.7161	−0.0716

Take, as an example, the spin-polarized charge densities of the GNR-A (3,4), which is shown in Fig. 2, from which it is easily found that the magnetic moment is mostly localized on its zigzag edge no matter the FM or AFM one. Only small amounts of the induced moments exist in the nearest neighbors of the zigzag edge, but no obvious moment can be found at the grain boundary and the armchair edge.

The FM configuration of GNR-A (3,4), shown in Fig. 2(a), is found to be in its ground state, exhibiting a one-dimensional (1D) FM coupling. Its local spin moment can be calculated by using the Bader method,[28] which is found to be about 1.2 μ_{B} per atom at the zigzag edge, and about 0.1 μ_{B} per atom at some nearby atoms, while all the other atoms have only negligible moments. Since hybrid GNR edges are not saturated by hydrogen or other elements, the dangling bonds at the zigzag edge atoms contribute a large amount to magnetic moment. Aside from that, the edge state composed of π electrons of zigzag edge atoms also contributes a small amount to magnetic moment. For a hydrogen-saturated GNR-A (3,4), it is found that the local spin moment is reduced greatly to about 0.2 μ_{B} per zigzag edge atom, indicating that the dangling bond in the bare hybrid GNR is totally spin polarized with its spin moment of about 1.0 μ_{B} per zigzag atom.

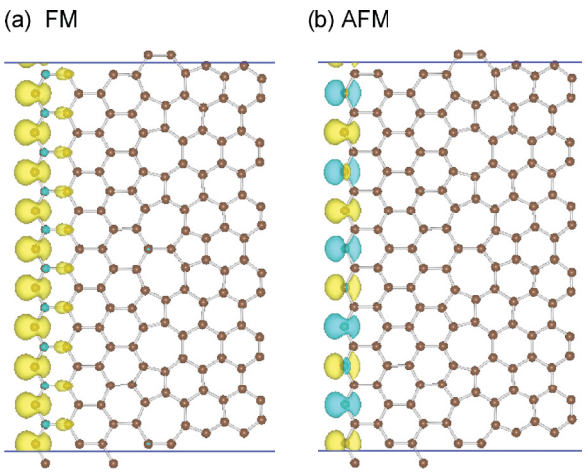

FIG. 2. (Color online) Spin-polarized charge densities of the GNR-A (3,4) in (a) the FM and (b) AFM configurations. Here, a $2 \times 1 \times 1$ supercell is used for calculation of the AFM state. The yellow and cyan represent the spin-up and -down charge densities, respectively.

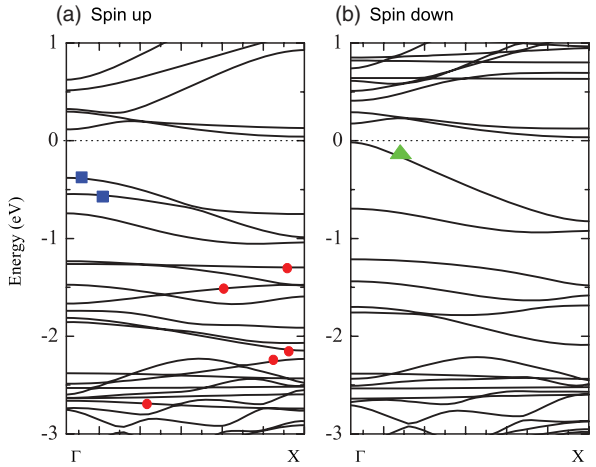

FIG. 3. (Color online) Spin-polarized band structures of the GNR-A (3,4). The red circles, blue rectangles, and green triangle represent the dangling bonds, edge state, and boundary defect state, respectively. Fermi energy is set to zero.

In order to deeply understand the FM origin of this hybrid GNR, we have calculated the spin-polarized band structure of the GNR-A (3,4) very carefully, which is shown in Fig. 3. By comparing the band structures near the Fermi energy for the GNR-A (3,4) with and without the hydrogen saturation, we can easily find that there are five dangling bonds in the range of about −3 to −1 eV of its valence band of spin-up channel, as indicated in Fig. 3(a), which exhibit the p_y character in the projected wave function at zigzag edge atoms. In contrast, there is no dangling bond in its spin-down channel, indicating that the five dangling bonds are totally spin polarized, contributing 5 μ_{B} in a unit cell of the FM GNR-A (3,4). This point can be also seen from its DOSs of a zigzag atom, shown in Fig. 4. We can find from the up panel of Fig. 4 that the p_y orbital is totally spin polarized, showing large spin-up DOSs between −3 and −1 eV.

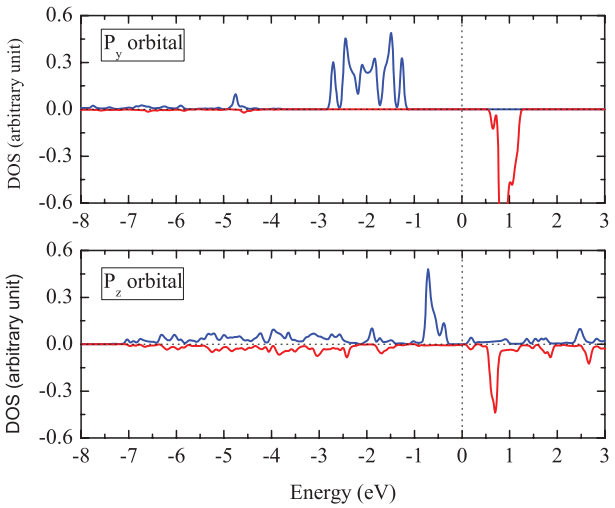

FIG. 4. (Color online) Spin-polarized density of states (DOSs) of one zigzag atom of the GNR-A (3,4). The up and down panels represent the p_y (dangling bond) and p_z (edge state) orbitals, respectively. The blue and red lines denote the spin-up and -down DOSs, respectively. Fermi energy is set to zero.

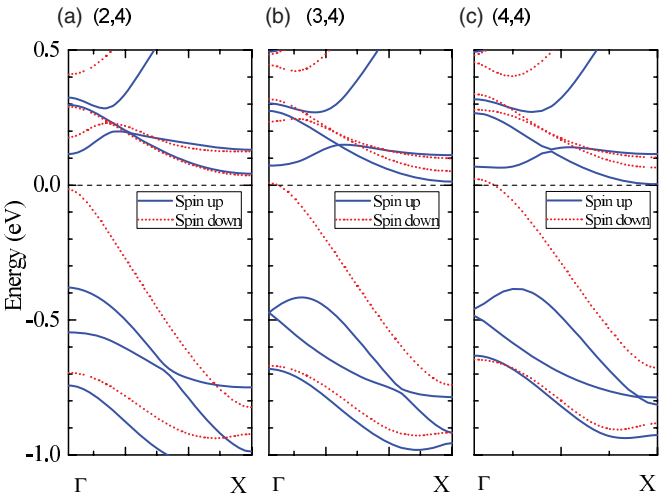

FIG. 5. (Color online) Spin-polarized band structures of the GNR-A (2,4), (3,4), and (4,4). The blue (solid) and red (dotted) lines represent the spin-up and -down bands, respectively. Fermi energy is set to zero.

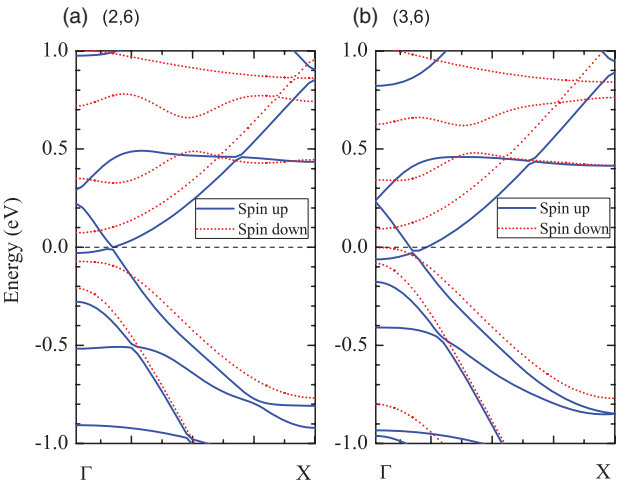

FIG. 6. (Color online) Spin-polarized band structures of the GNR-B (2,6) and (3,6). The blue (solid) and red (dotted) lines represent the spin-up and -down bands, respectively. Fermi energy is set to zero.

Besides, two edge states also exist in its spin-up channel, lying between about -1 and -0.3 eV, which are found to be mainly p_z character in the projected wave function at zigzag edge atoms, and are also totally spin polarized, as shown clearly in Figs. 3 and 4.

We have also studied the dependence of the spin-polarized band structure of the type-A structure on its width. The calculated results for the GNR-A (2,4), (3,4), and (4,4) are given in Fig. 5. Here, the GNR-A width is increased by only an additional zigzag chain from (2,4) to (4,4). It is interesting to find that the GNR-A (2,4) is a semiconductor with a small band gap of about 0.06 eV, as indicated in Fig. 5(a). In fact, the GNR-A (1,4) with the narrower width is also found to be a semiconductor, which is not mentioned here. When we add one more zigzag carbon chain from the GNR-A (2,4) to form the GNR-A (3,4) and (4,4), a spin-down valence band below the Fermi level of the GNR-A (2,4) is found to rise and cross the Fermi level by a little bit, finally making the GNR-A (4,4) metallic. Therefore, a semiconductor-metal (S-M) transition can happen when the zigzag chain part width of the GNR-A varies, which is induced by the quantum confinement effect of the small width.

More interestingly, it is found from Fig. 5 that there exists a wide energy range (from about -0.4 eV to Fermi energy), in which the energy band is totally spin polarized (as also indicated by the green triangle in Fig. 3). In other words, the type-A structure can exhibit an interesting half-metallic behavior in this wide range of energies, which is almost independent of its zigzag chain part width. It is found by analyzing the projected wave function that this spin-down band is mostly composed of the π orbitals at boundary defect atoms, which is, however, found to show a large dispersion because of the periodicity of boundary 5-7 defects in our model. Thus, this spin-down band could transport electrons well. This half-metallicity makes the hybrid GNRs very useful in the future application of spintronics.

B. Type-B and -C structures

Now, we turn to other two hybrid GNRs, i.e., the type-B and -C ones, which have two and one 5-7 defect in a unit cell of the boundary defects, as shown in Figs. 1(b) and 1(c), respectively. We have found by the DFT calculations that the ferromagnetism shown in type-A hybrid GNRs also appears in these two type-B and -C structures, indicating the robustness of the ferromagnetism of the hybrid GNRs, which is independent of the number of 5-7 defects in a unit cell of the grain boundary.

Take, as an example, the geometric structure of the GNR-B (3,6), which is shown in Fig. 1(b). In order to calculate its total energy in the AFM configuration, we have also used a $2 \times 1 \times 1$ supercell. However, we found that the AFM spin configurations of the GNR-B (1,6) and (2,6) are automatically converged to the FM ones, indicating that the AFM configuration is not stable right now and the FM state is their ground state. For a wider GNR-B (3,6), the total energy of its AFM configuration is found to be 0.04 eV per zigzag atom higher in energy than that of the FM one, which is similar to the type-A structures.

The spin-polarized band structures of the GNR-B (2,6) and (3,6) are given in Fig. 6, from which it is obviously seen that both of them are metallic. It is found that all the calculated GNR-B structures exhibit the metallic behavior even for the very narrow GNR-B (1,6), which is different from the GNR-A structures. The metallic property of the GNR-B structures is probably caused by their large lattice mismatch. On the other hand, their spin-polarized charge densities are very similar to those of the GNR-A structures, and are not mentioned here.

The obvious half-metallicity found in the type-A structures is not very obvious in the type-B ones. However, it can be found from Fig. 6 that for both the GNR-B (2,6) and (3,6), there is still a small energy range near the Fermi level, where the spin is totally polarized (spin up).

Finally, let us study the type-C structure, which has only one 5-7 defect in a unit cell at its boundary, shown in Fig. 1(c). Its lattice mismatch is about 6.70%, with its zigzag edge compressed and its armchair one elongated. We have found

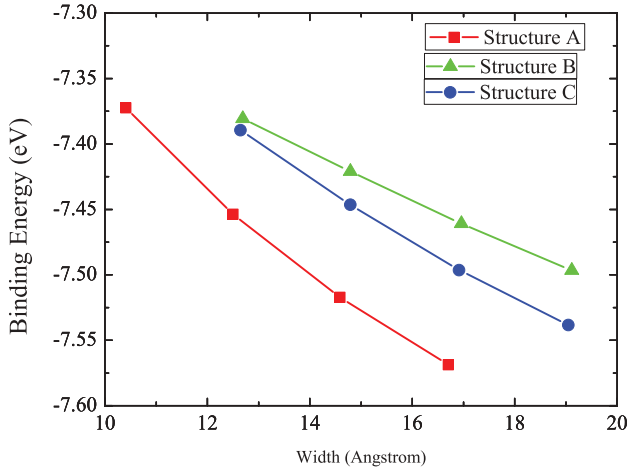

FIG. 7. (Color online) Dependence of the binding energies of the GNR-A, -B, and -C structures on the widths of their zigzag chain parts.

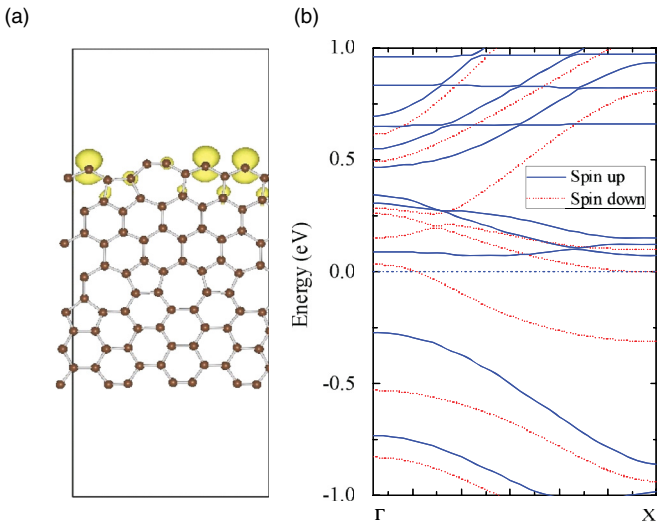

FIG. 8. (Color online) GNR-A (3,4) with the SW defect on its zigzag edge: (a) its geometrical structure and spin-polarized charge density, and (b) its spin-polarized band structure.

by the DFT calculations that its magnetic properties are still similar to those of the GNR-A and GNR-B, although it has a different topological 5-7 defect structure at its grain boundary. For example, the FM configuration is always the ground state of the GNR-C (1,6) to (4,6). The energy difference between their FM and AFM states is about 0.01 eV per zigzag atom, which is a little bit smaller than those of the GNR-A and GNR-B structures. The calculated band structures (not shown here) indicate that all the type-C structures are metallic due to the large lattice mismatch. In addition, the half-metallicity can still be found near the Fermi energy, although its energy range is also quite small.

C. Stability of the hybrid GNR with grain boundary

Now, it is interesting to discuss the relative stability of the different types of hybrid GNRs. In order to do so, we have calculated their binding energy E_b, defined as $E_b = (E_{tot} - n \times E_C)/n$, where E_{tot} and E_C are the total energies of the hybrid GNR and carbon atom, respectively, and n is the number of total atoms in a unit cell of the GNR. The calculated results are plotted in Fig. 7. It is obviously seen from Fig. 7 that all the hybrid GNRs have negative binding energies of about $-7.3 \sim -7.6$ eV, which are a little bit higher than that of the graphite (-7.9 eV), calculated by similar parameters. That means all these types of the hybrid GNRs are stable.

It is also found that their binding energies decrease with increasing their zigzag chain part widths, which is the same for all three types of the hybrid GNRs. It is because the edge atoms have large elastic energies, and they will occupy more and more weights in the system when the ribbon's width becomes smaller and smaller.

On the other hand, it can be also found from Fig. 7 that at the same width, the type-A structure has the lowest binding energy, indicating it is the most stable among the three types of hybrid GNRs, and the type-B structure has the highest one. That is because the former has the smallest lattice mismatch (-1.96%), while the latter has the largest one (-7.74%), leading to its higher binding energies.

D. Effects of defects at the zigzag edge of the type-A hybrid GNR

It is inevitable that some kinds of defects exist at the GNR's edges, such as the impurities, vacancies, and topological defects, etc., when the hybrid GNRs are synthesized in practice. Therefore, it is interesting to study their effects on the electronic and magnetic properties of the perfect hybrid GNRs. Here, we have considered only one kind of important topological defect at the zigzag edge of the type-A structure, which is the well-known Stone-Wales (SW) defect at the zigzag edge.

It is found that the edge reconstruction due to the SW defects at the zigzag edge is energetically favored, which could spontaneously take place at room temperatures.[29–32] Here, as an example, we have chosen a specific SW defect structure, called zz(57666), which contains only one SW defect at the zigzag edge in a unit cell of the GNR-A (3,4) structure, as shown in Fig. 8(a). It is seen clearly from Fig. 8(a) that there are three hexagons and one pair of pentagon and heptagon at the zigzag edge in one unit cell. The calculated spin-polarized charge density is also given in Fig. 8(a), showing clearly that the magnetic moments still exist at the zigzag edge atoms, although they are greatly reduced at the SW defect sites, which remain to be the FM coupling along the edge. The Bader charge analysis found that the local magnetic moments are all about 1.0 μ_B.

The calculated spin-polarized band structure of the defective GNR-A (3,4) is shown in Fig. 8(b). By comparing Fig. 8(b) with Figs. 3 or 5(b), it is shown that the SW defect makes the spin-down valence band nearest to the Fermi level rise up, crossing the Fermi level, and become less dispersive. In addition, the defective GNR-A (3,4) is obviously metallic now, but still keeping its half-metallicity in an energy range near the Fermi level, as shown in Fig. 8(b).

Therefore, it is naturally expected that increase of the SW defect concentration would further suppress the magnetic

moments at the zigzag edge but never kill them at all. For example, the local magnetic moments can appear on the zigzag edges of the GNR zz(5766), i.e., the defective ZGNR, at 50% SW defect concentration.[30] Only at the 100% SW defect concentration, i.e., for the ZGNR zz(57) structure, would all the magnetic moments and half-metallicity property disappear. That means the interesting physical properties of the hybrid GNRs can have good tolerance of the edge defects, especially at the low concentrations of SW defects. This is a very important characteristic for the experimental observations.

Finally, one may be much concerned with how the above hybrid GNRs could be produced in practice. Now, we want to give a short discussion on the important problem. It is now possible to produce graphene sheets by the chemical vapor deposition (CVD) on scales up to meters,[33–35] in which appearance of the polycrystallinity is almost unavoidable.[16] Therefore, we can first select some grain boundaries from the polycrystalline graphene sheet, which can then be cut along the selected grain boundary by using the different patterning methods, such as the *e*-beam lithography,[36] scanning tunneling lithography,[37] and chemical reactions with crystallographic selectivity,[38] in a simultaneous control of the crystallographic orientation (e.g., the zigzag and armchair edge directions) and the ribbon width with high precision,[37,39] creating finally a required hybrid GNR with a zigzag edge.

On the other hand, it is noted that the appearance of grain boundary is closely related to the surface adsorbates and substrate imperfections, etc.[16] In addition, there are a lot of chemical methods to produce the normal GNRs with a finite width. Therefore, probably, a periodical array of the impurity's nucleation sites could be prearranged on the copper foil, based upon which the traditional CVD method is then used to grow the hybrid GNRs with a required grain boundary and zigzag edge.

IV. CONCLUSIONS

Three kinds of hybrid GNRs are constructed by using different grain boundaries. The robust FM state is found to be the ground state in all of them due to their particular geometric structures. The FM coupling energy is found to be 0.01 $\sim$ 0.08 eV per zigzag edge atom, corresponding to a high FM Curie temperature.

Most of the hybrid GNRs are FM metals, except for some type-A structures with very small widths, in which a metal-semiconductor transition can happen when the number of their zigzag carbon chains reduces. But, two other GNR-B and GNR-C structures always show the metal properties due to their large internal strains, caused by the larger lattice mismatches at their grain boundaries. More interestingly, the half-metallicity is found in all the hybrid GNRs, especially in the type-A structures, where the energy range showing the half-metallicity reaches 0.4 eV, making them possibly useful in the future application in spintronics.

Finally, the binding-energy calculations and the study of the SW edge defect effects show that these hybrid GNRs could be stable, making them possibly synthesized in future experiments, and their fascinating properties, e.g., the ferromagnetism and half-metallicity, survive the existence of edge defect in them.

ACKNOWLEDGMENTS

This work is supported by the National Natural Science Foundation of China under Grants No. 10874067 and No. 11004094, specialized Research Fund for the Doctoral Program of Higher Education (20100091120008). We also acknowledge the support from the State Key Program for Basic Research of China through the Grants No. 2010CB630704 and No. 2011CB922100Q. Our DFT calculations are performed in the High Performance Computing Center of Nanjing University.

*zhoujian@nju.edu.cn
†Corresponding author: jdong@nju.edu.cn

[1] Y. B. Li, S. S. Xie, W. Y. Zhou, D. S. Tang, X. P. Zou, Z. Q. Liu, and G. Wang, Carbon **39**, 626 (2001).
[2] L. G. Cançado, M. A. Pimenta, B. R. A. Neves, G. Medeiros-Ribeiro, T. Enoki, Y. Kobayashi, K. Takai, K. I. Fukui, M. S. Dresselhaus, R. Saito, and A. Jorio, Phys. Rev. Lett. **93**, 047403 (2004).
[3] S. Dutta and S. K. Pati, J. Mater. Chem. **20**, 8207 (2010).
[4] V. Barone, O. Hod, and G. E. Scuseria, Nano Lett. **6**, 2748 (2006).
[5] Y. W. Son, M. L. Cohen, and S. G. Louie, Phys. Rev. Lett. **97**, 216803 (2006).
[6] H. Lee, Y.-W. Son, N. Park, S. Han, and J. Yu, Phys. Rev. B **72**, 174431 (2005).
[7] Y. W. Son, M. L. Cohen, and S. G. Louie, Nature (London) **444**, 347 (2006).
[8] E. J. Kan, Z. Y. Li, J. L. Yang, and J. G. Hou, Appl. Phys. Lett. **91**, 243116 (2007).
[9] E. J. Kan, X. J. Wu, Z. Y. Li, X. C. Zeng, J. L. Yang, and J. G. Hou, J. Chem. Phys. **129**, 084712 (2008).
[10] X. H. Zheng, X. L. Wang, T. A. Abtew, and Z. Zeng, J. Phys. Chem. C **114**, 4190 (2010).
[11] S. Dutta, A. K. Manna, and S. K. Pati, Phys. Rev. Lett. **102**, 096601 (2009).
[12] O. V. Yazyev and S. G. Louie, Nat. Mater. **9**, 806 (2010).
[13] J. Cervenka, M. I. Katsnelson, and C. F. J. Flipse, Nat. Phys. **5**, 840 (2009).
[14] A. R. Botello-Méndez, E. Cruz-Silva, F. López-Urías, B. G. Sumpter, V. Meunier, M. Terrones, and H. Terrones, ACS Nano **3**, 3606 (2009).
[15] A. N. Andriotis and M. Menon, Appl. Phys. Lett. **92**, 042115 (2008).
[16] P. Y. Huang, C. S. Ruiz-Vargas, A. M. van der Zande, W. S. Whitney, M. P. Levendorf, J. W. Kevek, S. Garg, J. S. Alden, C. J. Hustedt, Y. Zhu, J. Park, P. L. McEuen, and D. A. Muller, Nature (London) **469**, 389 (2011).
[17] Y. Liu and B. I. Yakobson, Nano Lett. **10**, 2178 (2010).
[18] J. Lahiri, Y. Lin, P. Bozkurt, I. I. Oleynik, and M. Batzill, Nat. Nanotechnol. **5**, 326 (2010).
[19] L. A. Jauregui, H. Cao, W. Wu, Q. K. Yu, and Y. P. Chen, Solid State Commun. **151**, 1100 (2011).

[20]F. Banhart, J. Kotakoshi, and A. V. Krasheninnikov, ACS Nano **5**, 26 (2011).
[21]O. V. Yazyev and S. G. Louie, Phys. Rev. B **81**, 195420 (2010).
[22]J. Cervenka and C. F. J. Flipse, Phys. Rev. B **79**, 195429 (2009).
[23]G. Kresse and J. Hafner, Phys. Rev. B **48**, 13115 (1993).
[24]G. Kresse and J. Furthmüller, Comput. Mater. Sci. **6**, 15 (1996).
[25]P. E. Blöchl, Phys. Rev. B **50**, 17953 (1994).
[26]G. Kresse and D. Joubert, Phys. Rev. B **59**, 1758 (1999).
[27]J. P. Perdew, K. Burke, and M. Ernzerhof, Phys. Rev. Lett. **77**, 3865 (1996).
[28]W. Tang, E. Sanville, and G. Henkelman, J. Phys.: Condens. Matter **21**, 084204 (2009).
[29]P. Koskinen, S. Malola, and H. Häkkinen, Phys. Rev. Lett. **101**, 115502 (2008).
[30]B. Huang, M. Liu, N. H. Su, J. Wu, W. H. Duan, B. L. Gu, and F. Liu, Phys. Rev. Lett. **102**, 166404 (2009).
[31]G. D. Lee, C. Z. Wang, E. Yoon, N. M. Hwang, and K. M. Ho, Phys. Rev. B **81**, 195419 (2010).
[32]J. N. B. Rodrigues, P. A. D. Gonçalves, N. F. G. Rodrigues, R. M. Ribeiro, J. M. B. Lopes dos Santos, and N. M. R. Peres, Phys. Rev. B **84**, 155435 (2011).
[33]X. S. Li, W. W. Cai, J. An, S. Kim, J. Nah, D. X. Yang, R. Piner, A. Velamakanni, I. Jung, E. Tutuc, S. K. Banerjee, L. Colombo, and R. S. Ruoff, Science **324**, 1312 (2009).
[34]X. S. Li, C. W. Magnuson, A. Venugopal, J. An, J. W. Suk, B. Y. Han, M. Borysiak, W. W. Cai, A. Velamakanni, Y. W. Zhu, L. F. Fu, E. M. Vogel, E. Voelkl, L. Colombo, and R. S. Ruoff, Nano Lett. **10**, 4328 (2010).
[35]S. Bae, H. Kim, Y. B. Lee, X. F. Xu, J. S. Park, Y. Zheng, J. Balakrishnan, T. Lei, H. R. Kim, Y. Song, Y. J. Kim, K. S. Kim, B. Özyilmaz, J. H. Ahn, B. H. Hong, and S. Iijima, Nat. Nanotechnol. **5**, 574 (2010).
[36]M. Y. Han, B. Özyilmaz, Y. B. Zhang, and P. Kim, Phys. Rev. Lett. **98**, 206805 (2007).
[37]L. Tapasztó, G. Dobrik, P. Lambin, and L. P. Biró, Nat. Nanotechnol. **3**, 397 (2008).
[38]P. Nemes-Incze, G. Magda, K. Kamarás, and L. P. Biró, Nano Res. **3**, 110 (2010).
[39]L. P. Biró and P. Lambin, Carbon **48**, 2677 (2010).